Chapter 6
Full-Field Analysis of the Strain-Induced Crystallization in Natural Rubber

S. Charlès and J. -B. Le Cam

Abstract The strain-induced crystallization is generally considered to be responsible for the excellent properties of natural rubber, especially its remarkable crack growth resistance.

The crystallinity of rubber is classically studied by using X-ray diffraction (XRD). The XRD technique gives access to the crystallinity but also information of paramount importance on the crystalline phase structure (Rajkumar, et al., Macromolecules 39:7004, 2006), chain orientation (Toki, et al., Rubber Chemistry and Technology 42:956-964, 2004), kinetics of crystallization (Trabelsi, Macromolecules 36:9093–9099, 2003), non-exhaustively. However, this method provides this information at one point.

Recently, a new method has been proposed in (Le Cam, Strain 5:54, 2003) for determining the crystallinity, from infrared thermography-based surface calorimetry. In the case of heterogeneous heat source field and large deformations, the method requires combining digital image correlation and infrared thermography. In the present study, this methodology is applied to measure full heat source field in a stretched rubber specimen. The crystallinity as well as its spatial distribution is characterized.

Keywords Strain-induced crystallization · Natural rubber · Infrared thermography · Surface calorimetry · Digital image correlation

6.1 Introduction

Strain-induced crystallization (SIC) is classically mentioned to explain the remarkable properties of natural rubber compared to non-crystallizing elastomers [9–11]. Since its discovery by Katz in 1925 [12], many experimental methods have been used to explore more deeply this phenomenon, such as stress relaxation [13], Raman Spectroscopy [14], birefringence [15], or nuclear magnetic resonance [16]. However, X-ray diffraction remained the most used method to investigate SIC.

While this method gives access to the crystallinity, it also provides information on crystallites morphology and the crystallographic structure. Nevertheless, this kind of information is provided at a single point. This limitation can induce issues in case of crystallinity heterogeneity, such as at a crack tip [17].

Since the SIC phenomena is a strong exothermal phenomenon [18], a new method has been proposed in [8] and validated in [19].

In this study, this method is used to measure crystallinity at several materials points simultaneously in an unfilled natural rubber specimen submitted to a uniaxial tensile loading.

6.2 Experimental Setup

In the present study, an unfilled natural rubber is considered. The specimen geometry corresponds to a thin rectangular specimen, as shown in Fig. 6.1.

S. Charlès (✉) · J. -B. Le Cam
IPR (Institut de Physique de Rennes) – UMR 6251, Univ Rennes, CNRS, Rennes, France
e-mail: sylvain.charles@univ-rennes1.fr

S. L. B. Kramer et al. (eds.), *Thermomechanics & Infrared Imaging, Inverse Problem Methodologies, Mechanics of Additive & Advanced Manufactured Materials, and Advancements in Optical Methods & Digital Image Correlation, Volume 4*, Conference Proceedings of the Society for Experimental Mechanics Series, https://doi.org/10.1007/978-3-030-86745-4_6

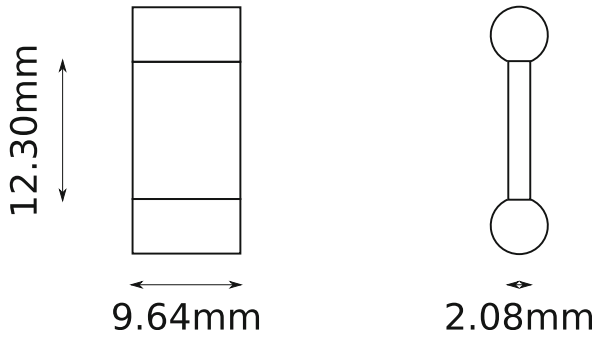

Fig. 6.1 Specimen geometry

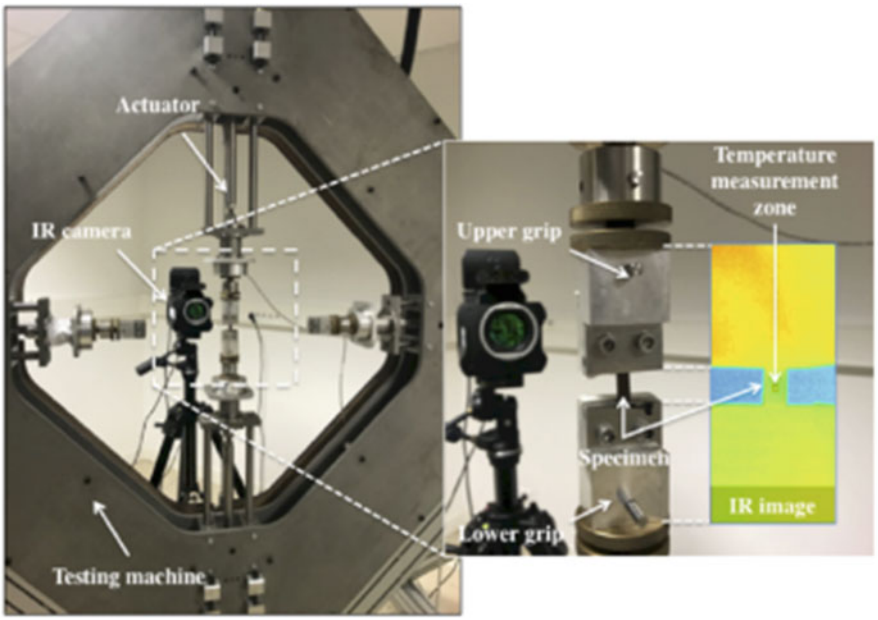

Fig. 6.2 Experimental setup

Figure 6.2 presents an overview of the experimental setup used for this study. The mechanical test is performed using a home-made biaxial testing machine. This machine is composed of four independent RCP4-RA6C-I-56P-4-300-P3-M (IAI) electrical actuators. They are driven by a CON-CA-56P-I-PLP-2-0 controller and four PCON-CA (IAI) position controllers. An in-house LabVIEW program piloted these actuators. This machine enables us to stretch symmetrically the specimen. Therefore, the specimen center is motionless.

The mechanical loading applied consists in three loading/unloading uniaxial cycles. The maximal displacement and loading rate of each actuator are set at 36 mm and 150 mm/min, respectively, which corresponds to a maximal stretch of about 7.

Temperature measurements are performed by using a FLIR infrared camera equipped with a focal array of 640x512 pixels and detectors operating in wavelengths between 1.5 and 5.1 µm. The integration time is equal to 2700 µs, and the acquisition frequency is equal to 20 Hz. The calibration of camera detectors is performed with black body using a one-point NUC procedure at this acquisition frequency. The thermal resolution, or noise equivalent temperature difference (NETD), is equal to 20 mK for a temperature range between 5 and 40 °C. The spatial resolution of the thermal field is equal to 300 µm/px. The infrared camera is switched on several hours before the test in order to stabilize its internal temperature. To deduce the temperature field from R thermography, the emissivity of the material must be known. In the present study, a value of 0.94 has been taken.

6.3 Motion Compensation Technique

Since the specimen undergoes large deformations during the test, material points move from pixel to pixel. Determining the heat source variation and thus the crystallinity at any point requires knowing the temperature variation at any point and any time.

For that purpose, a motion compensation technique has to be used. In the present study, the temperature measurement is performed at the median section of the specimen. The strain field is assumed to be homogeneous, which means that no displacement occurs in the stretch direction in this zone, only displacement along the width due to the cross-section contraction. An algorithm has been developed to follow the borders of the specimen in the IR images and therefore to evaluate the displacement of the points due to the cross-section contraction.

6.4 Crystallinity Measurement

Evaluating the crystallinity requires several steps. Once the motion compensation method has been performed, and the temperature evolution obtained, the heat diffusion equation is first applied. For that purpose, several assumptions are done; they are recalled in [8].

The total heat source produced by the material during the test is expressed as follows:

$$S = \rho C_p \left(\dot{\theta} + \frac{\theta}{\tau} \right) - k \Delta_{2D} \theta$$

with S the heat source produced by the material, θ the temperature variation, ρ the mass density of the material at its undeformed state, C_p the calorific capacity of the material, and k the thermal conductivity of the material.

The second step consists in predicting the heat source S_{el} if no crystallization occurs by using a polynomial form of the heat source. This is possible by considering the heat source variations before the crystallization starts.

$$S_{el} = C_1(I_1 - 3) + C_2(I_1 - 3)^2 + C_3(I_1 - 3)^3$$

with I_1 the first invariant of the Cauchy-Green tensor and C_1, C_2, and C_3 are three parameters to be identified. Figure 6.3 represents both the heat source measured and the heat source predicted using the polynomial form at a single point. The two vertical lines delimit the time range (or the strain range) where the identification was performed.

The difference between the predicted and measured curves at high strains is due to the heat produced by the crystallization phenomenon. Once the heat source due to SIC is identified, the crystallinity is obtained by integrating the heat source due to SIC over the time:

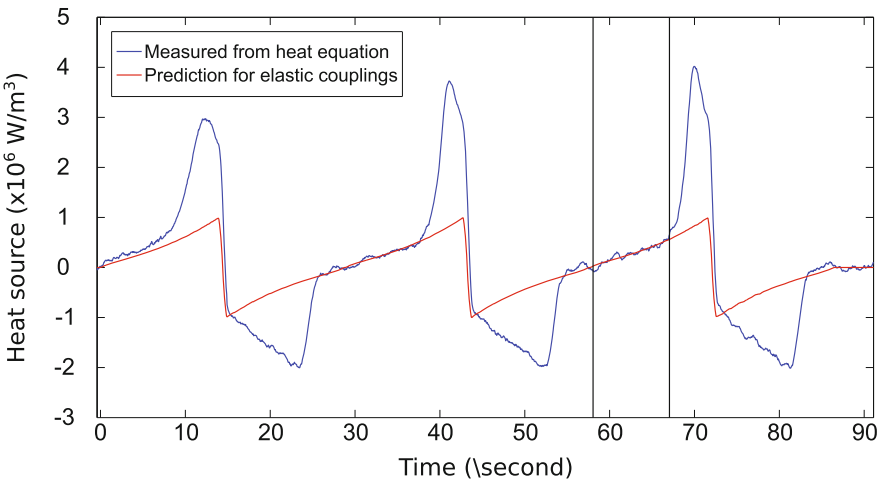

Fig. 6.3 Heat source during the full mechanical test

$$\chi = \int_0^t \frac{S_{\text{cryst}}}{\Delta H} dt$$

with χ the crystallinity level, S_{cryst} the heat source due to SIC phenomenon and ΔH the fusion enthalpy.

6.5 Highlighting Crystallinity Heterogeneities

Results will be more precisely detailed and analyzed during the presentation, especially the heterogeneity detected in terms of crystallinity from one point to another.

Acknowledgments The authors thank the National Center for Scientific Research (MRCT-CNRS and MI-CNRS), Rennes Metropole and Region Bretagne for financially supporting this work and the Michelin Company for providing the specimens. Authors also thank Dr. Mathieu Mirroir, Mr. Vincent Burgaud, and Mr. MickaelLefur for having designed the biaxial tensile machine.

References

1. Bunn, C.W.: Proc. R. Soc. London, Ser. **180**, 40–66 (1942)
2. Takahashi, Y., Kumano, T.: Macromolecules. **37**, 4860 (2004)
3. Immirzi, A., Tedesco, C., Monaco, G., Tonelli, A.E.: Macromolecules. **38**, 1223 (2005)
4. Rajkumar, G., Squire, J.M., Arnott, S.: Macromolecules. **39**, 7004 (2006)
5. Toki, S., Sics, I., Ran, S.F., Liu, L.Z., Hsiao, B.S., Murakami, S., Tosaka, M., Kohjiya, S., Poompradub, S., Ikeda, Y., Tsou, A.H.: Rubber Chem. Technol. **42**, 956–964 (2004)
6. Toki, S., Fujimaki, T., Okuyama, M.: Polymer. **41**, 5423–5429 (2000)
7. Trabelsi, S., Albouy, P.-A., Rault, J.: Macromolecules. **36**, 9093–9099 (2003)
8. Le Cam, J.-B.: Strain. **5**, 54 (2018)
9. Trabelsi, S., Albouy, P.-A., Rault, J.: Macromolecules. **36**, 7624–7639 (2003)
10. Hamed, G.R., Kim, H.J., Gent, A.N.: Rubber Chem. Technol. **69**, 807–818 (1996)
11. Lake, G.J.: Rubber Chem. Technol. **68**, 435–460 (1995)
12. Katz, J.R.: Naturwissenschauften. **13**, 410–416 (1925)
13. Gent, A.N.: Trans. Faraday Soc. **28**, 625–628 (1954)
14. Healey, A.M., Hendra, P.J., West, Y.D.: Polymer. **37**, 4009–4024 (1996)
15. Treloar, L.R.G.: Trans. Faraday Soc. **37**, 84–97 (1941)
16. Tanaka, Y.: Rubber Chemistry and Technology. **74**, 355–375 (2001)
17. Rublon, P., et al.: Eng. Fract. Mech. **123**, 59–69 (2014)
18. Göritz, D., Müller, F.H.: Kolloid-Zeitschrift und Zeitschriftfür Polymere. **241**, 1075–1079 (1970)
19. Le Cam, J.-B., Albouy, P.-A., Charlès, S.: Review of Scientific Instruments. **91**, 044902 (2020)